biblio.ugent.be

The UGent Institutional Repository is the electronic archiving and dissemination platform for all UGent research publications. Ghent University has implemented a mandate stipulating that all academic publications of UGent researchers should be deposited and archived in this repository. Except for items where current copyright restrictions apply, these papers are available in Open Access.

This item is the archived peer-reviewed author-version of: Impact of vacuum-induced surface freezing on inter- and intra-vial heterogeneity

Authors: Oddone I., Van Bockstal P.J., De Beer T., Pisano R.

In: European Journal of Pharmaceutics and Biopharmaceutics 2016, 103: 167-178

To refer to or to cite this work, please use the citation to the published version:

Oddone I., Van Bockstal P.J., De Beer T., Pisano R. (2016)
Impact of vacuum-induced surface freezing on inter- and intra-vial heterogeneity. European Journal of Pharmaceutics and Biopharmaceutics 103 167-178

DOI: 10.1016/j.ejpb.2016.04.002

Submitted for the publication on *European Journal of Pharmaceutics and Biopharmaceutics*

Impact of vacuum-induced surface freezing on inter- and intra-vial heterogeneity

Irene Oddone,[a] Pieter-Jan Van Bockstal,[b] Thomas De Beer,[b] Roberto Pisano [a,*]

(a) Department of Applied Science and Technology, Politecnico di Torino, corso Duca degli Abruzzi 24, 10129 Torino (Italy)

(b) Laboratory of Pharmaceutical Process Analytical Technology, Department of Pharmaceutical Analysis, Ghent University, Ottergemsesteenweg 460, B-9000 Gent (Belgium)

Corresponding author:

roberto.pisano@polito.it

Tel: +39 011 090 4679

Fax: +39 011 090 4624

Abstract

This paper aims to study the impact of freezing on both within-batch (inter-vial) and within-product (intra-vial) heterogeneity. This analysis has been carried out using two freezing protocols, the conventional shelf-ramped method and the Vacuum Induced Surface Freezing, and placebo formulations containing both crystallizing (mannitol) and amorphous (lactose and sucrose) excipients. The freezing conditions (i.e., the temperature of freezing, the temperature and time of the equilibration phase, and the filling volume) were found to have a dramatic impact on both the within-batch and the within-product homogeneity. Overall, we observed that the control of freezing can effectively minimize the variability in product characteristics, and moisture content, within the same batch. In addition to more uniform production, the control of freezing was found to be fundamental to achieve a more uniform product than that produced by the shelf-ramped freezing method. The influence of the freezing protocol on the crystallization process of mannitol was also investigated, showing that the temperature of freezing plays a key role in the formation of the mannitol polymorphs.

Chemical compounds studied in this article

Mannitol (PubChem CID: 96011), Lactose (PubChem CID: 6134), Sucrose (PubChem CID: 5988).

Keywords: Freeze-drying, batch heterogeneity, freezing, mannitol, Raman spectroscopy

Introduction

Freeze-drying is widely used in the pharmaceutical industry to preserve product stability during shipment and storage. During the development of the freeze-drying cycle, attention has to be given to freezing since it is responsible for both within-batch and the within-product variability. The former is partially caused by the stochastic nature of freezing, which makes individual vials behave differently during drying as they have different product properties [1, 2]. Recently, various methods (alternative to the shelf-ramped freezing) have been proposed to make this process less unpredictable [3-14]. Among these include the following: electrofreezing [4], ultrasound [5-8], depressurization method [9] and ice fog technique [10-11]. All these methods were found to give a dramatic reduction in cycle duration and improve the homogeneity of the batch as a whole, thus ensuring similar product characteristics in all the vials of the batch. However, most of the methods proposed for the control of freezing have various limitations related to, e.g., the requirement of additional equipment, modification of pre-existing freeze dryers, and scalability. Beside these engineering issues, it is also important to investigate the effect of the freezing method on the product structure. In fact, although the effect of the controlled freezing on the duration of the lyophilization cycle was demonstrated over the last decade [2], little attention has been paid to its impact on within-vial heterogeneity and to the selection of appropriate process conditions that allows the satisfaction of aesthetic quality requirements. In this context, this paper aims to deeply investigate the impact of controlled freezing techniques on both within-batch (inter-vial) variability and within-product (intra-vial) variability. The Vacuum Induced Surface Freezing (VISF) method [12-13] was taken into consideration because of its ease of application; the conventional shelf-ramped freezing was

used as reference for the comparison. As concerns the VISF method, it must be noted that the original method proposed by Kramer *et al*. [12] has been modified as shown in Oddone et al. [14] so as to avoid undesired phenomena (boiling and blow-up) that can produce aesthetic defects. This result was achieved by the shut-off of the valve between the condenser and the drying chamber as soon as the desired vacuum has been reached. It must be noted that the results obtained in this study are not specific to VISF, but can be generalized to the other controlled freezing methods proposed in literature where the control of freezing is achieved by introducing a perturbation on the top surface of the product.

The attention of this work was particularly focused on intra-vial heterogeneity as it can have a direct impact on the stability of active pharmaceutical molecules, promoting undesired phenomena, e.g., protein aggregation [15-16]. Another aspect of interest is the effect of controlled freezing on the crystallization of some excipients commonly used in pharmaceutical formulations; to give you an example, mannitol after drying can be present either as an amorphous product or as three different crystalline forms: α, β and δ [17-18]. The hemihydrate form was more recently reported by Yu *et al.* and Nunes *et al.* [19-20]. Not all these forms can effectively protect the active molecules against deactivation [21] and it has been found to have an impact on the stability of the product during its storage [22-24]. For example, the hemihydrate mannitol, if present in the lyophilized product, is not stable during storage, but is transformed into anhydrous crystalline mannitol (δ polymorph) by releasing its hydrate water within the amorphous phase, presumably containing the active pharmaceutical ingredient, increasing the rate of degradation. Of course, any transformation during storage is undesired and thus this phenomenon, when possible, has to be avoided [20, 25]. It follows that the

selection of the freezing method, and process conditions as well, is an important task to be considered during cycle development.

In this paper, the impact of the freezing method (controlled vs. uncontrolled) on the morphology of mannitol-based formulations was investigated using both X-ray diffractometric analysis and Raman spectroscopy. The application of this last method is particularly helpful to increase the understanding of the mechanisms at the basis of mannitol crystallization as it allows a more detailed description of the structure of the lyophilized product, giving information about potential variations in mannitol polymorphs along the cake.

Materials and Methods

Product preparation and freezing

Batches of 70 vials (ISO 80462 6R) were filled with solutions of mannitol 5 and 10% (w/w), lactose 5% (w/w), and sucrose 5% (w/w), products purchased from Sigma Aldrich (Italy), in water for injection (Fresenius Kabi, Italy). The formulations were filtered with a 0.2 μm pore size filter and prepared under laminar flow cabinet (V-100, Azbil Telstar, Terrassa, Spain); igloo stoppers (type 1319 4432/50/ Westar, West Pharmaceutical Services, Terrassa, Spain) were used as closures. The batches of vials were loaded directly on the shelf using hexagonal arrangement and processed in a pilot-scale freeze-dryer (LyoBeta 25 by Telstar, Terrassa, Spain). The formulations were tested upon both uncontrolled and controlled freezing.

The controlled freezing method is a modification of the Vacuum Induced Surface Freezing method [12-13] as proposed in a previous work [14]. The liquid is first equilibrated at T_n for

about 45 min and, then, the pressure is reduced to a given value, which is product-specific (130 Pa for mannitol 5%, 150 Pa for mannitol 10%, 110 Pa for lactose 5%, and 150 Pa for sucrose 5%), for 1 min [12]. The equilibration time is selected by monitoring the temperature of the liquid and looking for the minimum time needed to homogenize the temperature of all the vials of the batch. The pressure decrease promotes the initiation of the freezing process, which proceeds from the top surface to the bottom of the liquid. After 1 min at this low pressure, the pressure within the chamber is released to the atmospheric value as fast as possible, in order to avoid aesthetic problems due to boiling and blow-up of the frozen layer. Subsequently, the temperature of the heat transfer fluid (T_f) is decreased as fast as possible (about 1 °C min^{-1} in the case of our equipment) to a value (T_m) below the onset of ice melting and held for about 1 h. This stabilization phase allows the formation of large ice crystals and prevents melting back. To complete the freezing of the product, T_f is finally decreased to −45°C and held for at least 1 h.

As one of the objectives of the work is to investigate the effect of freezing conditions on inter- and intra-vial heterogeneity, cycles were carried out varying both T_n and T_m as shown in Table 1. Furthermore, the effect of the vial type (a-vial, $D_{v,i}$=14 mm; b-vial, $D_{v,i}$ =22 mm) and the filling volume was also investigated, see Table 2. This last set of tests was carried out using a fixed freezing protocol (T_n=−5 °C and T_m=−10 °C). As a comparison, cycles using the shelf-ramped freezing were also carried out; in this case T_f was held at −22 °C for 3 h, decreased to −45 °C, and held at this temperature for further 2 h.

Primary Drying

For all the cycles carried out with mannitol, the primary drying was carried out at 10 Pa, while the temperature of the heat transfer fluid was automatically adjusted by the *LyoDriver* control system [26-28]. During this step, the product temperature at the bottom of the vial (T_b) and the mass-transfer resistance of the dried cake lug to the vapour flow (R_p) were monitored using the pressure rise test technique coupled with the dynamic parameters estimation (DPE+) algorithm [29]. For tests 9-12 of Table 1 and the all cycles shown in Table 2, primary drying was carried out at 10 Pa and −10°C.

Within-batch heterogeneity

The within-batch heterogeneity was evaluated at the end of primary drying in terms of difference between the onset and the offset time of the pressure ratio curve [14, 30], hereafter referred to as onset-offset time (see Figure 1). The pressure ratio curve is calculated considering the ratio between the thermo-conductive sensor (Pirani, type PSG-101-S, Infcon, Bad Ragaz, Switzerland) and the capacitive sensor (Baratron, type 626A, MKS Instruments, Andover, MA) of which the freeze dryer is equipped.

Within-product heterogeneity

The lyophilized samples were characterised upon morphology, residual water content, and polymorph formation. These analysis were carried out using mannitol-based formulations as model product.

Internal structure of the cake

The internal structure of the cake was assessed using a Scanning Electron Microscope (SEM, FEI type, Quanta Inspect 200, Eindhoven, Netherlands). SEM images were taken at various

positions along the sample in order to obtain a quantitative estimation of within-vial heterogeneity. This quantitative analysis was done in terms of size (d_p) and distribution of the pore size, and was carried out using the software Image J.

Residual moisture content

The residual moisture content of the samples was investigated by Karl Fisher analysis (Coulometer DL-32; Mettler Toledo, USA). This analysis was performed at the end of primary drying on 20 samples collected from the central part of the batch.

Characterization of mannitol-based formulations

For mannitol-based formulations, X-ray diffractometry (XRD, X-pert Powder type, PANalytical, Almelo, Netherlands) was used to identify the polymorphic state of the lyophilized samples. XRD measurements were done in the reflection mode, within 5-60° as 2θ range, using a mask of 10 mm opening and slits of ½°; data were acquired at each 0.02°. Analysis of the diffractograms was done using X-Pert Data Analysis program; the X-ray diffraction patterns acquired were compared with those of the reference materials (α, β and δ-anhydrous mannitol). For each cycle, the XRD characterization was replicated for 5 samples. Furthermore, cycles 1-4 were also measured by Raman spectroscopy. Raman spectra were collected at four different positions: top surface of the lyophilized cake, surface closed to the bottom of the container, and two different positions of the central part of the cake. For each position, we have collected 5 Raman spectra. At the end of the cycle, the lyophilized cake was cut and divided into four pieces and placed under the non-contact Raman probe for off-line measurements. This analysis was done for 5 samples. Raman spectra were collected with a Raman Rxn1 spectrometer (Kaiser Optical Systems, Ann Arbor, MI, USA) equipped with a

785 nm Invictus NIR diode laser. The spectra were recorded with a resolution of 4 cm^{-1} using a laser power of 400 mW. For each spectrum an exposure time of 15 seconds and 3 accumulations were used. HoloGRAMS^{TM} data collection software (Kaiser Optical Systems, Ann Arbor, MI, USA) and Matlab software (version 7.1, The Mathworks Inc., Natick, MA) were used for data collection and data transfer. Due to the large amount of Raman spectra, a suitable chemometric tool was necessary for the analysis of these spectra. In particular, SIMCA software (Version 13.0.3, Umetrics, Umeå, Sweden) was used to perform principal component analysis (PCA) to determine the mannitol polymorph content. The use of PCA for the analysis of Raman spectra is thoroughly described by De Beer *et al*. [22]. Off-line collected Raman spectra were introduced into one data matrix (**D**). All spectra were pre-processed by Standard Normal Variate (SNV) normalization and centered. The spectral region of interest for mannitol polymorph identification was 850-1200 cm^{-1}. PCA decomposes an orthogonal bilinear data matrix, while sequentially producing principal components (PCs) to explain maximum variation:

$$\mathbf{D} = \mathbf{T}\mathbf{P}^{\mathbf{T}} + \mathbf{E} = \mathbf{t_1}\,\mathbf{p_1'} + \mathbf{t_2}\,\mathbf{p_2'} + \ldots + \mathbf{t_Q}\,\mathbf{p_Q'} + \mathbf{E}$$

where **T** is the **M**×**Q** score matrix, **P** the **N**×**Q** loading matrix, **E** the **M**×**N** model residual matrix, **Q** the selected number of PCs and N the number of collected spectra at M wavelengths [31]. Each PC is composed by two vectors, the score vector **t** and the loading vector **p**. For each spectrum the score vector contains a score value. This value represents the position of the spectrum towards the other spectra for that specific component. The loading vector displays the spectral features in the original spectra captured by this PC. These unique, abstract, and orthogonal PCs are helpful for gathering the diverse sources of variation present in the data. However, these PCs do not necessarily correspond to the true underlying factors causing the

data variation, but are orthogonal linear combinations of them, since each PC is obtained by maximizing the amount of variance it can explain [32].

Results and Discussion

Impact of freezing conditions on within-batch heterogeneity

The within-batch heterogeneity was evaluated in relation to the primary drying time, considering the onset-offset time of the pressure ratio curve. As can be seen in Table 3, cycles with controlled freezing showed the shortest onset-offset time. As general trend, we observed that the onset-offset time of cycles with shelf-ramped freezing was 40% longer than that observed for cycles with controlled freezing. This result confirmed what has been already shown by Oddone *et al*. [14]; the controlled freezing makes the batch of vials more uniform in relation to their drying behaviour.

As concerns cycles with controlled freezing, we have also evaluated the effect of freezing conditions, T_n and T_m, on product and process performances. This analysis was carried out using mannitol 5% as model formulation. As can be seen in Table 3, the onset-offset time of controlled cycles (Tests 2-6 in Table 1) was significantly shorter (from 35% up to 60%) than that observed for uncontrolled freezing (Test 1). This result was observed for all the controlled cycles, but it was less marked for Test 5 (about 10%). This was likely due to the partial melting back of the frozen product that, as confirmed by the visual inspection of the samples, occurred during its equilibration at T_m. It must be remarked that Test 5 was carried out at the highest value of T_m (=−5 °C) and, thus, this temperature was likely too high to impede the melting back event. As a consequence, a part of the solution was frozen later on and the freezing of that part occurred as in a conventional shelf-ramped freezing cycle. This result was also confirmed by

SEM analyses, which showed that Test 5 gave the smallest pore size (i.e., about 80 μm) among the cycles with controlled freezing. Besides, this result was confirmed by comparing Tests 5 and 3. In fact, the only difference in the case of Test 3 was the lower value of T_m (i.e., −10 °C instead of −5 °C with test 5), which was enough low to avoid the melting back of the frozen solution (again confirmed by visual inspection), producing very large pores (about 120 μm). The addition of an annealing step, after a short holding at T_m=−5 °C, promoted again a much more open structure (about 140 μm) and greater uniformity (Test 6). The melting back did not occur and the onset-offset time was reduced of about 40%, with respect to the conventional freezing, and of about 30% with respect to Test 5. Furthermore, we observed that the controlled freezing method allowed to produce more uniform batches independently of the formulation used, see Tests 7 and 8 for mannitol 10% and Tests 9 and 10 for lactose 5%. The onset-offset times of Tests 8 and 10 were again significantly shorter (50 and 63% respectively) in comparison with those carried out using the uncontrolled freezing (Tests 7 and 9). As further confirmation of these results, the residual moisture of 20 vials, sampled from the central part of the batch, was measured at the end of the primary drying phase. The results of this analysis are shown in Figure 2 for the uncontrolled (Test 1) and the controlled freezing (Test 3). The two distributions were characterized by similar mean values (about 4%), but different values of standard deviation. In particular, the moisture distribution of samples produced by the controlled freezing had the lowest standard deviation, 0.68 % vs. 1.63 %; the cumulative distributions also showed that the fraction of vials, having residual moisture lower than 5%, was 98% for the controlled freezing and only 85% for the uncontrolled freezing. These results seem to confirm that the controlled freezing produces more homogeneous batches, inducing the nucleation event in all the vials of the batch within narrow ranges of temperature and time.

Results in Table 3 also showed that there was not a clear relationship between the temperature at which freezing was induced, T_n, and the within-batch heterogeneity. As shown in Table 3, the onset-offset time changed with T_n, but there was not any monotonic dependence. These variations in the onset-offset time might be due to temperature gradients over the batch of vials. In fact, the selection of the stabilization time, needed to equilibrate the product temperature at T_n, was done by monitoring the product temperature (through thermocouples) of vials placed in the central part of the batch. It is therefore possible that the selected time, i.e. 45 min, was not long enough to complete the temperature equilibration for edge-vials, thus promoting the freezing at different temperature for edge- and central vials. This is particularly true for laboratory equipment where the contribution of the side-wall radiation to the heat transfer is important.

Impact of freezing conditions on within-vial heterogeneity

Effect of filling volume, T_n, and T_m

As a first step we have analysed the effect of filling volume on intra-vial heterogeneity. Figure 3 shows the internal structure of samples produced using the same freezing conditions and vials, but increasing filling volume (D, F and G in Table 2). It can be observed that D samples showed the most uniform structure with respect to that observed for F and G samples. These last two samples presented a thin, very compact layer close to the top surface of the cake, while the rest of the product was characterized by a more open structure with the porosity that changed with the position into the vial; large pores and a dendritic structure was observed in the central portion of the cake, while spherical and smaller pores were present close to the top and to the bottom of the cake. This within-vial heterogeneity was likely due to a partial freezing

of the liquid in the case of high filling volume. This hypothesis was confirmed by Figure 4a which shows D, F and G samples as observed immediately after the pressure reduction; in this picture the formation of a frozen layer close to the top surface can clearly be identified for only the F and G samples (having high fill volume), which was responsible for the compact porous structure shown in Figure 3a-d. By contrast, the compact porous layer at the bottom of F samples (see Figure 3g) was due to the formation of a second freezing front (close to the bottom of the container) that faded in during the stabilization phase at $T_m = -10$ °C; this last step allows the promotion of the crystal growth and inhibits the melting back of ice, see Figure 4b. During this phase, the formation of filaments of ice was observed in the core of the liquid being frozen, see Figure 4c. These filaments generated the dendritic structure observed in the central portion of F and G samples, see Figure 3b,c,e,g. It follows that the ice crystal growth was different across different manufacturing conditions; e.g., if we use high filling volume, the temperature gradient is significant along the liquid being frozen, influencing the formation and the growth of ice crystals. As general guideline, we can conclude that the smaller the filling volume was (i.e., D samples), the more uniform the internal porous structure was. Besides, we observed that the freezing process of all those samples having similar filling volume was not influenced by the type of vial used. This fact can be appreciated from the visual observation of the freezing for samples B-E (9 mm as product height) and C-F (17 mm as product height), see Figure 4.

SEM micrographs were analysed by using the software Image J in order to evaluate size and distribution of the pores, see Figure 3. This analysis showed similar values of d_p close to the top and the bottom of the cake, while significantly different pore sizes were observed in the central part. For those images that contain a dendritic structure, the value of d_p was estimated referring to a surface that is orthogonal to the crystal growth.

The second part of the analysis was focused on the effect of freezing conditions (namely T_n and T_m) on within-vial heterogeneity; this study was carried out for mannitol 5%, see tests 1-6 in Table 1. The SEM micrographs of these samples, taken at three positions along the cake (top, centre and bottom), along with the pore size, as estimated by Image J software, are shown in Figure 5. As can be seen in Figure 5 (pictures d-f), Test 2 (that was carried out at the highest value of T_n) showed more marked variations in pore size moving from the top surface of the cake toward the bottom of the container. In the case of this test, in fact, T_n had the highest value and likely was not low enough to promote the freezing throughout the entire filling volume; as a consequence, a thin layer of ice was formed at the top surface of the product, while the remaining liquid froze as soon as T_f was decreased to −10 °C, producing a dendritic structure. A similar behaviour was observed in Figure 4b,c. The most uniform structure (among those cycles carried out using the controlled freezing) was found for test 4 with T_n= −10 °C and T_m= −10 °C. For test 4, pore size and shape were nearly uniform along the product height (d_p=100 μm) with the exception of the thin, compact structure at the top surface of the cake that is typical for all samples produced using the controlled freezing. If we use an intermediate value between tests 2 and 4 (see Test 3, T_n= −5 °C), marked variations can again be observed in pore size moving from top toward the bottom of the product; the highest d_p was observed in the central part of the product (about 120 μm), while pores at the bottom container showed an average value of d_p of about 105 μm. It is possible to hypothesise that if T_n is higher than −10 °C (for a filling depth of 10 mm), freezing could not occur through the entire volume of liquid, but a part of the liquid remained unfrozen. The remaining liquid froze during the subsequent stabilization phase. As general guideline, we can conclude that the pore size increased as T_n increased. In particular, we observed that the average value of d_p, as measured in the central

part of the cake, was 150 μm for Test 2 (T_n=+5 °C), 120 μm for Test 3 (T_n= −5 °C) and 105 μm for Test 4 (T_n= −10 °C). As concerns the within-vial heterogeneity, it is not clear if the heterogeneity was due to different extent of supercooling or differences in the growth of ice crystals. Oddone *et al*. [33] showed that the temperature gradient along the product being frozen is modest during the pressure decrease, and this gradient is nearly zero during the nucleation event. This result is valid when the liquid depth is smaller than 1 cm. In the case of low filling volumes, we can thus hypothesize that the intra-vial heterogeneity is likely due to changes in the growth of ice crystals. The situation was totally different for high filling volumes; in this last case, the pressure reduction promotes the freezing event only in the top part of the product, while the underneath part remains liquid and freezes later on. Therefore, in this last case the within-vial heterogeneity was likely due to different extent of supercooling.

The other process parameter of interest is the temperature of the stabilization phase, T_m.. Tests 3 and 5 were carried out using the same value of T_n= −5 °C, but changing T_m; −10 °C and −5 °C respectively. As shown in Figure 5 (pictures g-i and o-q), the pore size d_p of samples produced by Test 5 was significantly lower than that observed for Test 3, 80 μm vs. 120 μm. We hypothesized that this result was due to the fact that after stabilization, the solution was not completely frozen and thus freezes as soon as the temperature of the heat transfer fluid was reduced to −45 °C. A further test was carried out, i.e. Test 6, in order to investigate the effect of an annealing treatment after the controlled freezing. As can be seen in Figure 5, pictures (r-t), the annealing made it possible to reduce within-vial heterogeneity and also promoted the growth of ice crystals, 140 μm for Test 6 vs. 80 μm for Test 5. As further support to pore size and distribution analysis, the resistance to mass transfer (as a function of the thickness of the dried layer) was estimated through the pressure rise test technique. To this regard, in the case

of tests 5 and 6, it was found that a variation of about 40 μm had an impact on R_p vs. L_{dried} of about 40% (see Figure 6b). Pisano *et al*. [34] combined the shelf-ramped freezing with the annealing and observed a similar reduction in the values of R_p vs. L_{dried}. Nevertheless, it has also been observed that the homogeneity of the batch has not been significantly improved by the annealing as this treatment can partially compensate the heterogeneity due to the stochastic freezing method.

Figure 6a shows the R_p values obtained for tests 2-4 which were carried out using the controlled freezing and different values of T_n. The results are coherent with the pore size analyses shown in Figure 5; to give you an example, Test 2 gave the biggest pore dimension and the lowest values of R_p vs. L_{dried}. By contrast, Test 4 gave the smallest pore size and the highest values of R_p vs. L_{dried}. In particular, we observed that variations in pore size of about 50 μm produced variations in R_p values of 45%. Furthermore, the trends of R_p vs. L_{dried} changed for L_{dried} higher than 2 mm; this result suggests the formation of a similar structure closed to the top surface of the product. This observation is in agreement with what was observed by SEM micrographs analysis of the cake. in Figure 6 R_p values of test 1, carried out with uncontrolled nucleation, are also reported as a control.

Figure 5 (pictures a-c) also shows the internal structure of samples obtained through the conventional shelf-ramped freezing. It can be observed that uncontrolled freezing gave the smallest pore size (about 12 μm), but a more uniform distribution with respect to that observed for samples produced through the controlled freezing. If the more uniform structure was an advantage from the point of view of active ingredients stability, the very compact porous structure gave the highest resistance to mass transfer (as shown in Figure 6b) and thus was a disadvantage in terms of drying time and energy consumption.

The best solution, which gave an acceptable intra-vial product homogeneity and large pores (thus short cycle duration), was Test 4, which uses the controlled freezing method and the lowest values of T_n and T_m, both equal to −10 °C.

To verify the results obtained for the intra-vial homogeneity of a mannitol model formulation, two additional tests containing sucrose (5%, w/w) were carried out (tests 11-12 of Table 1). Figure 7 shows that also in the case of amorphous solutions the controlled nucleation promoted the formation of bigger ice crystals, about 140 μm (figures a-b, test 11), in comparison with an uncontrolled cycle, about 90 μm (figures d-f, test 12), even if the differences found in the case of these tests were less marked in comparison with mannitol solutions (12 μm vs. 120 μm for $T_n = -5$°C). The structure along the product of the controlled cycle was found homogeneous in agreement with the temperature of nucleation ($T_n = -5$°C) and height of product in vial (about 1 cm) chosen for this test.

XRD and Raman analysis: polymorphic state

The role of the manufacturing conditions on the crystallization of mannitol has already been addressed in the literature [35]; this interest is motivated by the fact that the various mannitol polymorphs (α, β, and δ) show different thermodynamic stability, which can have an impact on the final characteristics of the active pharmaceutical ingredients. The thermodynamically stable form of mannitol is the β polymorph, while the α and δ ones are metastable [36]. It follows that it is fundamental to control the crystallization of mannitol in order to guarantee the stability of lyophilized drugs. For this reason, we have investigated the impact of freezing conditions, and in particular of the Vacuum Induced Surface Freezing method, on the formation of mannitol polymorphs.

Figure 8 and Figure 9 show the results of XRD characterization for lyophilized samples of mannitol 5% as produced using various freezing protocols. Figure 8, in particular, shows the XRD spectra obtained for samples produced using the shelf-ramped freezing (Test 1in Table 1) and the characteristic peaks of anhydrous mannitol polymorphs (α, β, and δ). We can observe the formation of both β and δ with traces of α. By contrast, mannitol samples produced through the controlled freezing method varied in polymorph composition depending on the process conditions. Samples produced in Tests 2, 3 and 5 were prevalently made of δ mannitol. Test 4 gave substantially only β and traces of α. A similar composition was observed for Test 6, where an annealing treatment was added. Mannitol 10% (Test 8) was made mainly of δ (as reported by Kim *et al.* [37]) independently of the freezing protocol used.

As a further test, we used Raman spectroscopy to investigate more thoroughly the variations in mannitol polymorph formation as the freezing protocol is modified. In Figure 10A and Figure 10B respectively the score scatter plot and the loading line plot are shown for the spectra collected at the bottom, the inside and the outside of the cakes. The spectra recorded at the top of each sample were excluded, because the intra-vial distribution of polymorphs in the cakes was uniform, except near the top surface of the cake. Spectra collected at the top of each sample often contained slightly higher amounts of α and δ mannitol in comparison with the spectra recorded in the other regions of the same cake. The spectra collected in Tests 2, 3 and 4 tend to group in the score plot, while the spectra from Test 1 were more spread. This result indicates that the mannitol composition was more uniform for the controlled freezing protocol than that observed for the shelf-ramped freezing. After comparison with pure mannitol polymorph reference spectra (Figure 10C), specific peaks could be identified in the loading plot. The peaks pointing upwards in the loading plot of PC1 matched δ mannitol (887 cm^{-1}, 1052 cm^{-1}, 1094

cm^{-1} and 1145 cm^{-1}), while the peaks in the opposite direction matched the β polymorph (876 cm^{-1}, 1037 cm^{-1}, 1118 cm^{-1} and 1134 cm^{-1}) (Figure 10B). The scores of PC1, explaining 66.8% of the variation in the dataset, are displayed on the horizontal axis of the score plot. Therefore, spectra situated close to the right-side of the score plot contained more δ mannitol (and less β mannitol) as opposed to those situated near the left-side. Based on this, samples obtained at T_n= −5 °C (Test 3) clearly contained the highest amount of δ mannitol (Figure 10A). On the other hand, the content of δ mannitol formed at T_n= −10 °C (test 4) was much lower, because the spectra collected from the samples obtained during this test are situated at the far left side of the score plot (Figure 10A). Here, the polymorph content corresponds to the peaks pointing in the negative direction of the loading plot of PC1, identified as the β polymorph. These findings were also confirmed by the individual spectral analysis, indicating that at T_n of −10 °C almost pure β mannitol was formed. In the loading plot of PC2 δ mannitol (upwards directed peaks; 875 cm^{-1},1052 cm^{-1}, 1094 cm^{-1} and 1145 cm^{-1}) and α mannitol (downwards directed peaks; 886 cm^{-1},948 cm^{-1}, 1033 cm^{-1} and 1129 cm^{-1}) could be identified (Figure 10B). The scores of PC2, explaining 17.5% of the variation, are plotted along the vertical axis of the score plot. The spectra at the bottom of the score plot contain a higher amount of the α polymorph, those at the top contain a higher amount of δ mannitol. The spectra obtained at T_n= +5°C (test 2) were located at the bottom of the score plot, indicating that these cakes contained more α mannitol in comparison with the samples nucleated at a lower temperature (Figure 10A). Analysis of the individual spectra confirmed the presence of traces of α mannitol in the cakes. The high amount of δ mannitol present in the samples obtained at T_n= −5°C, Test 3, was already detected by PC1 and is confirmed in PC2 (Figure 10A). The presence of hemihydrate mannitol was not detected (neither by X-Ray Diffraction nor by Raman Spectroscopy) for any of the

freezing conditions investigated. The formation of mainly β polymorph (instead of instable δ [36]) well distributed within the cake in addition to the good intra-vial product homogeneity make the operating conditions of controlled freezing applied in Test 4 eligible for an optimal application of this control method.

The effect of controlled freezing on the formation of mannitol polymorphs have not previously been addressed in literature. The above results give additional information to the effect of manufacturing conditions on the solid state of lyophilised mannitol; slow cooling rate were found to promote a mixture of δ- (predominant) and α-forms (minor) [38], rapid cooling generates a mixture of α- (predominant) and δ-forms (minor), and the addition of an annealing step promote the formation of the stable β-form.

Conclusions

This study shows that the control of freezing can improve the within-batch homogeneity with respect to the conventional shelf-ramped freezing. This result can be achieved acting on the freezing temperature, T_n, and the holding temperature, T_m. Even if there was not a clear relationship between T_n and the within-batch heterogeneity, more uniform batches (with respect to the conventional freezing) were observed independently of T_n.

We also observed that the control of freezing promoted the formation of larger crystals of ice than those observed for the conventional shelf-ramped freezing. Besides, the within-product heterogeneity was found to be dependent on a number of process parameters: T_n, T_m, and the filling volume. As general guidelines, the within-product homogeneity was promoted by low values of T_n and of the filling volume. By contrast, the influence of T_m was minor, unless its value was so high to promote the melting back of the frozen solution. A further improvement

of both within-batch and within-product homogeneity could be obtained by the addition of the annealing treatment. It must be noted that all these results are not specific to the VISF method, but can likely be generalized to all those controlled freezing method proposed in literature where the freezing is induced by a perturbation on the top surface of the product.

A similar behaviour was observed for both crystallizing (i.e., mannitol) and amorphous excipients (i.e., lactose and sucrose). The above results can thus be generalized and are likely valid for the other excipients commonly used in lyophilization science.

In addition to product morphology, we also investigated the impact of the control of freezing on the crystallization process of mannitol, showing that the freezing conditions (T_n and T_m) can dramatically impact of the type of mannitol polymorph obtained after lyophilization, and on its distribution within the product as well.

List of symbols

D	data matrix
d_p	average pore size diameter (μm)
$D_{v,i}$	internal vial diameter (m)
E	residual matrix
L_{dried}	dry layer thickness (m)
M	number of wavelengths
N	number of collected spectra
p	loading vector
P	loading matrix
P_c	chamber pressure (Pa)
Q	number of principal components
R_p	resistance of the dried layer to vapour flow (m s^{-1})
t	score vector
T	score matrix
T_f	temperature of the heating fluid (°C)
T_b	product temperature at the bottom of the product (°C)
T_m	holding temperature after the induction of nucleation (°C)
T_n	holding temperature before the induction of nucleation (°C)

Abbreviations

DPE+	Dynamic Parameters Estimation
KF	Karl Fisher

PC	Principal Component
PCA	Principal Component Analysis
PRT	Pressure Rise Test
SEM	Scanning Electron Microscopy
VISF	Vacuum Induced Surface Freezing
XRD	X-Ray Diffraction

References

1. M.J. Pikal, S. Rambhatla, R. Ramot, The impact of the freezing stage inlyophilization: effects of the ice nucleation temperature on process design and product quality, Am. Pharm. Rev. 5 (2002) 48–53.

2. J.A. Searles, J.F. Carpenter, T.W. Randolph, The ice nucleation temperature determines the primary drying rate of lyophilization for samples frozen on a temperature-controlled shelf, J. Pharm. Sci. 90 (2001) 860–871.

3. J.C. Kasper, W.F. Friess, The freezing step in lyophilization: physico-chemical fundamentals, freezing methods and consequences on process performance and quality attributes of biopharmaceuticals, Eur. J. Pharm. Biopharm. 78 (2011) 248–263.

4. W. Rau, Eiskeimbildung durch Dielektrische Polarisation, Verlag der Zeitschrift für Naturforschung, 6 (1951) 649–657.

5. T. Inada, X. Zhang, A. Yabe, K. Yoshiyuki, Active control of phase change from supercooled water to ice by ultrasonic vibration, Part 1: Control of freezing temperature, Int. J. Heat and Mass Transfer. 44 (2011) 4523–4531.

6. X. Zhang, T. Inada, A. Yabe, S. Lu, Y. Kozawa, Active control of phase change from supercooled water to ice by ultrasonic vibration, Part 2: Generation of ice slurries and effect of bubble nuclei, Int. J. Heat and Mass Transfer. 44 (2001) 4533–4539.

7. M. Saclier, R. Peczalski, J. Andrieu, A theoretical model for ice primary nucleation induced by acoustic cavitation, Ultrason. Sonochem. 17 (2010) 98–105.

8. K. Nakagawa, A. Hottot, S. Vessot, J. Andrieu, Influence of controlled nucleation by ultrasounds on ice morphology of frozen formulations for pharmaceutical proteins freeze-drying, Chem. Eng. Process. 45 (2006) 783–791.

9. B.M. Rampersad, R.R. Sever, B. Hunek, T.H. Gasteyer, Freeze-dryer and method of controlling the same, U.S. Patent 8240065 B2 (2010).

10. S. Rambhatla, R. Ramot, C. Bhugra, M.J. Pikal, Heat and mass transfer scale-up issues during freeze drying, Part 2: Control and characterization of the degree of supercooling. AAPS PharmSciTech. 5 (4), 2004, article no. 58.

11. S. Patel, C. Bhugra, M. Pikal, Reduced pressure ice fog technique for controlled ice nucleation during freeze-drying, AAPS PharmSciTech. 10 (2009) 1406–1411.

12. M. Kramer, B. Sennhenn, G. Lee, Freeze-drying using vacuum-induced surface freezing, J. Pharm. Sci. 91 (2002) 433–443.

13. J. Liu, T. Viverette, M. Virgin, M. Anderson, P. Dalal, A study of the impact of freezing on the lyophilization of a concentrated formulation with a high fill depth, Pharma. Develop. Technol. 10 (2005) 261–272.

14. I. Oddone, R. Pisano, R. Bullich, P. Stewart, Vacuum Induced nucleation as a method for freeze-drying cycle optimisation, Ind .Eng. Chem. Res. 53 (2014) 18236–18244.

15. B.H. Peters, F. Molnár, J. Ketolainen, Structural attributes of model protein formulations prepared by rapid freeze-drying cycles in a microscale heating stage, Eur. J. Pharm. Biopharm. 87 (2014) 347–356.

16. K. Nakagawa, W. Murakami, T. Hatanaka, Redistribution of Protein Biological Activity in a Freeze-Dried Cake, Drying. Technol. 31 (2013) 102–111.

17. A. Burger, J.O. Henck, S. Hetz, J.M. Rollinger, A.A. Weissnicht, H. Stottner, Energy/temperature diagram and compression behavior of the polymorphs of D-mannitol, J. Pharm. Sci. 89 (2000) 457–468.

18. H. Bauer, T. Herkert, M. Bartels, K.A. Kovar, P.C. Schmidt, Investigations on polymorphism of mannitol/sorbitol mixtures after spray drying using differential scanning calorimetry, X-ray diffraction and near infrared spectroscopy, Pharm. Ind. 62 (2000) 231–235.

19. L. Yu, N. Milton, E.G. Gorleau, D.S. Mishra, R.E. Vansickle, Existence of a mannitol hydrate during freeze-drying and practical implications, J. Pharm. Sci. 88 (1999) 196–198.

20. C. Nunes, R. Suryanarayanan, C.E. Botez, P.W. Stephens, Characterization and crystal structure of D-mannitol hemihydrate, J. Pharm. Sci. (2004) 2800–2809.

21. R. Pisano, V. Rasetto, A.A. Barresi, F. Kuntz, D. Aoude-Werner, L. Rey, Freeze-drying of enzymes in case of water-binding and non-water-binding substrates. Eur. J. Pharm. Biopharm. 85 (2013) 974–983.

22. T.R.M. De Beer, M. Allesø, F. Goethals, A. Coppens, Y. Vander Heyden, H. Lopez De Diego, J. Rantanen, F. Verpoort, C. Vervaet, J.P. Remon, W.R.G. Baeyens, Implementation of a process analytical technology system in a freeze-drying process using Raman spectroscopy for in-line process monitoring, Anal. Chem. 79 (2007) 7992–8003.

23. T.R.M. De Beer, P. Vercruysse, A. Burggraeve, T. Quinten, J. Ouyang, X. Zhang, C. Vervaet, J.P. Remon, W.R.G. Baeyens, In-line and real-time process monitoring of a freeze

drying process using Raman and NIR Spectroscopy as complementary Process Analytical Technology (PAT) tools, J. Pharm. Sci. 98 (2009) 3430–3446.

24. W. Cao, C. Mao, W. Chen, H. Lin, S. Krishnan, N. Cauchon, Differentiation and quantitative determination of surface and hydrate water in lyophilized mannitol using NIR spectroscopy, J. Pharm. Sci. 95 (2006) 2077–2086.

25. C. Ahlneck and G. Zografi, The molecular basis of moisture effects on the physical and chemical stability of drugs in the solid state, Int. J. Pharm. 62 (1990) 87–95.

26. D. Fissore, R. Pisano, S.A. Velardi, A.A. Barresi, M. Galan., PAT tools for the optimization of the freeze-drying process, ISPE Pharm. Eng. 29 (2009) 58−70.

27. R. Pisano, D. Fissore, S.A. Velardi, A.A. Barresi, In-line optimization and control of an industrial freeze-drying process for pharmaceuticals, J. Pharm. Sci. 99 (2010) 4691−4709.

28. R. Pisano, D. Fissore, S.A. Velardi, A.A. Barresi, In-line and off-line optimization of freeze drying cycles for pharmaceutical products, Drying. Technol. 31 (2013) 905−919.

29. D. Fissore, R. Pisano, A.A. Barresi, On the methods based on the Pressure Rise Test for monitoring a freeze-drying process, Drying. Technol. 29 (2011) 73−90.

30. S. Passot, I.C. Tréléa, M. Marin, M. Galan, G.J. Morris, F. Fonseca, Effect of controlled ice nucleation on primary drying stage and protein recovery in vials cooled in a modified freeze-dryer, J. Biomech. Eng. 131 (2009) 074511−5.

31. L. Zhang, M. J. Henson, S.S. Sekulic, Multivariate data analysis for Raman imaging of a model pharmaceutical tablet, Anal. Chim. Acta. 545 (2005) 262−278.

32. A. De Juan, R. Tauler, Chemometrics applied to unravel multicomponent processes and mixtures: Revisiting latest trends in multivariate resolution, Anal. Chim. Acta. 500 (2003) 195−210.

33. I. Oddone, D. Fulginiti, A.A. Barresi, S. Grassini, R. Pisano. Non-invasive temperature monitoring in freeze-drying: control of freezing as a case study, Drying Technol. 33 (2015) 1621-1630.

34. R. Pisano, D. Fissore, A.A. Barresi, P. Brayard, P. Chouvenc, B. Woinet. Quality by design: Optimization of a freeze-drying cycle via design space in case of heterogeneous drying behavior and influence of the freezing protocol, Pharm. Dev. Technol. 18 (2013)280-295.

35. X. Liao, R. Krishnamurthy, R. Suryanarayanan. Influence of processing conditions on the physical state of mannitol. Implications in freeze-drying, Pharm. Research. 24 (2006) 370−376.

36. P. Gorth. Chemical Crystallography, Part Three, Aliphatic and Aromatic Hydrocarbon Compounds, Wilhelm Engelmann, Leipzig, 1910.

37. A. Kim, M. Akers, S. Nail, The physical state of mannitol after freeze-drying: Effects of mannitol concentration, freezing rate and non-crystallising cosolute, J. Pharm. Sci. 87 (1998) 931−935.

38. A. J. Cannon, E. H. Trappler. The influence of lyophilisation on the polymorphic behavior of mannitol, PDA J. Pharm. Sci. Technol. 54 (2000) 13−22.

List of Figures

at T_n = −5°C and (d-f, test 12 of Table 1). (Right graphs) The profile of d_p along the cake is shown, where 0 mm refers to the bottom of the container.

Figure 8: X-ray diffraction spectra of lyophilised mannitol 5% (using the uncontrolled freezing, Test 1) and the references spectra for α, β, and δ mannitol.

Figure 9: X-ray diffraction spectra of tests 2-6 in which (*) indicates α peaks and (•) δ peaks; the remaining peaks correspond to β polymorph.

Figure 10: Score scatter plot (A) and Loading line plot (B) for the Raman spectra collected at the bottom, the inside, and the outside of the cakes and Raman reference spectra of pure mannitol polymorphs (C). Data refer to 5 samples and 5 replication for each position.

List of Tables

Table 1

Test	*Solution*	*Nucleation type*	T_n, °C	T_m, °C	*Annealing,* °C	P_c, Pa
1	Mannitol 5%	Conventional	–	–	–	10
2	Mannitol 5%	Controlled	+ 5	–10	–	10
3	Mannitol 5%	Controlled	–5	–10	–	10
4	Mannitol 5%	Controlled	–10	–10	–	10
5	Mannitol 5%	Controlled	–5	–5	–	10
6	Mannitol 5%	Controlled	–5	–5	–10	10
7	Mannitol 10%	Conventional	–	–	–	10
8	Mannitol 10%	Controlled	+5	–10	–	10
9	Lactose 5%	Conventional	–	–		10
10	Lactose 5%	Controlled	–5	–10		10
11	Sucrose	Conventional	–	–	–	10
12	Sucrose	Controlled	–5	–10	–	10

Table 2

Sample	Internal Diameter, mm	Product height, mm
A	a	5
B		9
C		17
D	b	7
E		9
F		17
G		23

Table 3

Test	*Onset-offset range, h*	*Difference with respect to uncontrolled nucleation, %*
1	4.5	/
2	1.8	60
3	3	35
4	2.2	50
5	4	10
6	2.7	40
7	10	/
8	5	50
9	8.6	/
10	3.2	63

Figure 1

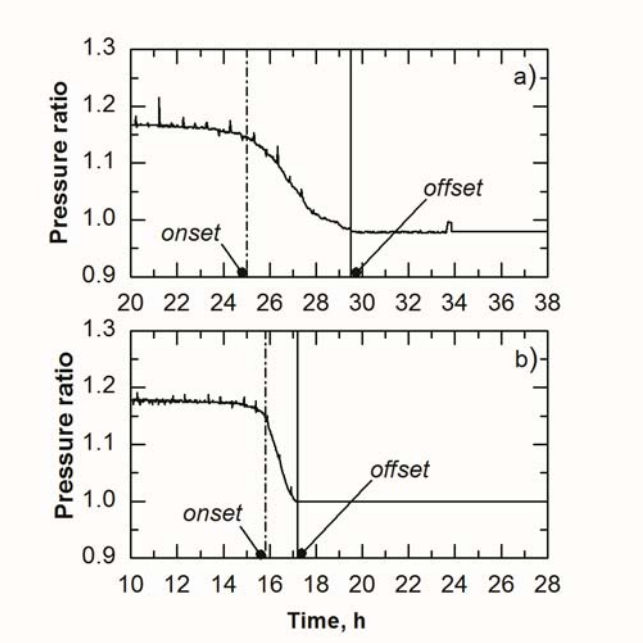
a)
b)
Pressure ratio
Pressure ratio
onset
offset
onset
offset
1.3
1.2
1.1
1.0
0.9
20 22 24 26 28 30 32 34 36 38
10 12 14 16 18 20 22 24 26 28
Time, h

Figure 2

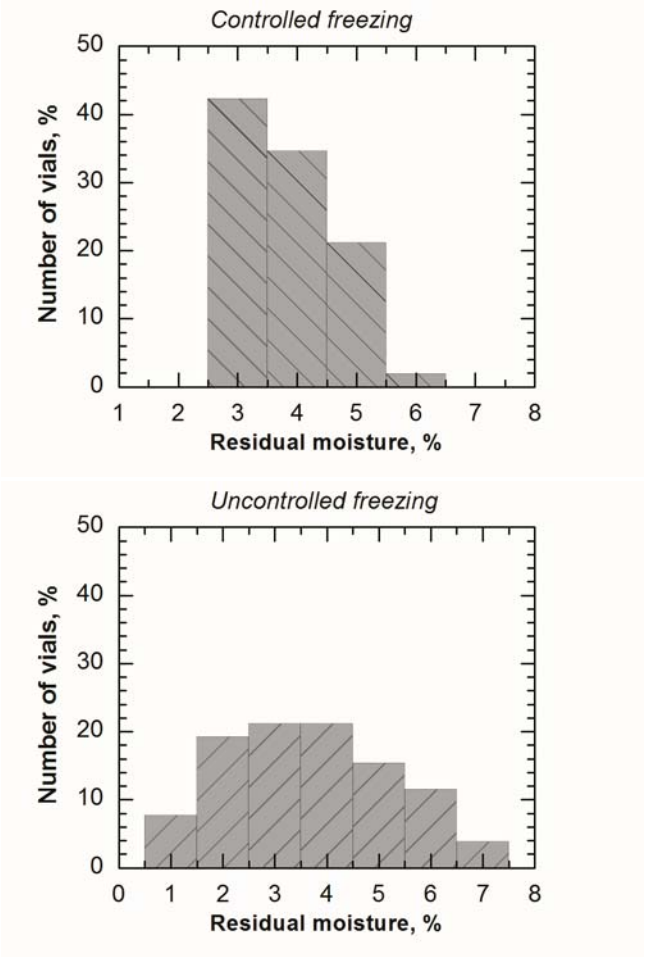
Controlled freezing
Number of vials, %
Residual moisture, %
Uncontrolled freezing
Number of vials, %
Residual moisture, %

Figure 3

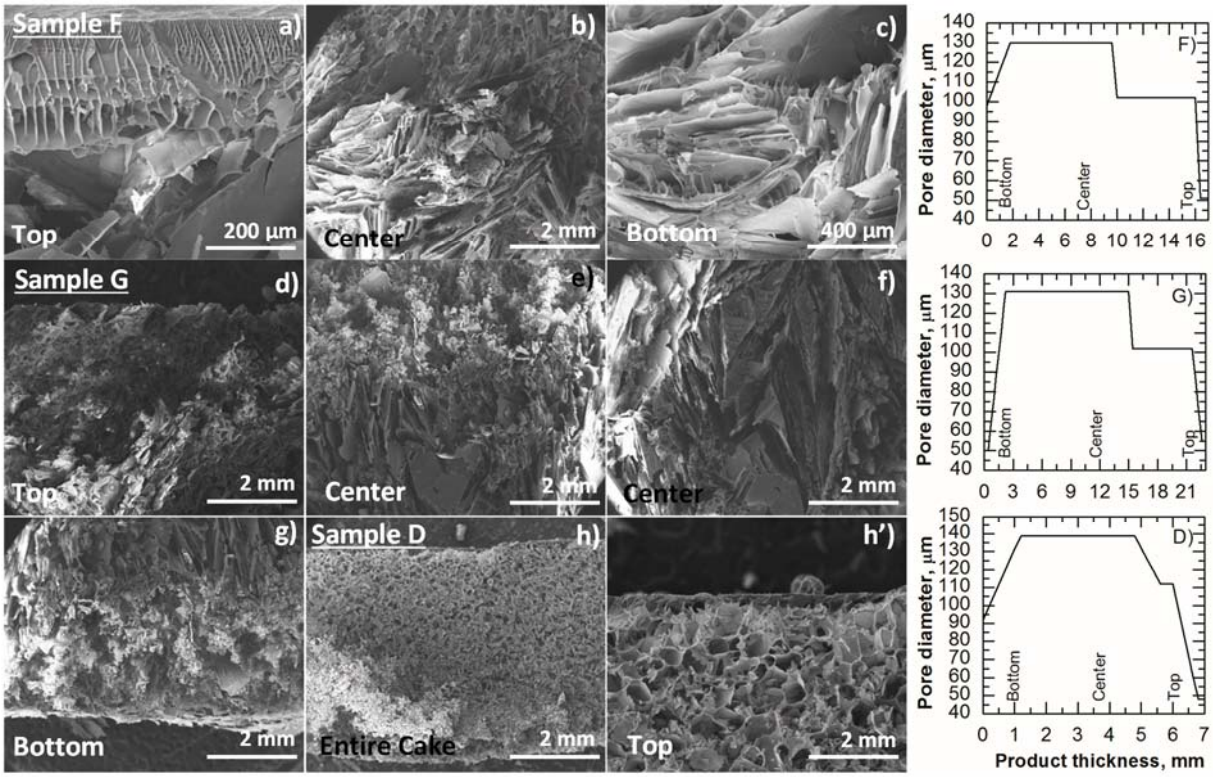
Sample F
a)
Top
200 µm
b)
Center
2 mm
c)
Bottom
400 µm
Sample G
d)
Top
2 mm
e)
Center
2 mm
f)
Center
2 mm
g)
Bottom
2 mm
Sample D
h)
Entire Cake
2 mm
h')
Top
2 mm
F)
G)
D)
Pore diameter, µm
Bottom
Center
Top
Product thickness, mm

Figure 4

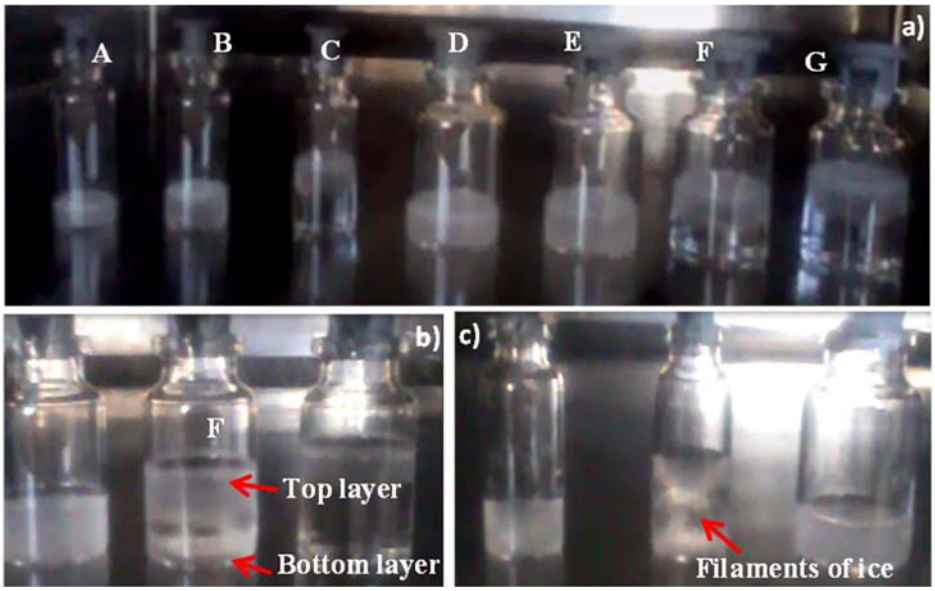

Figure 5

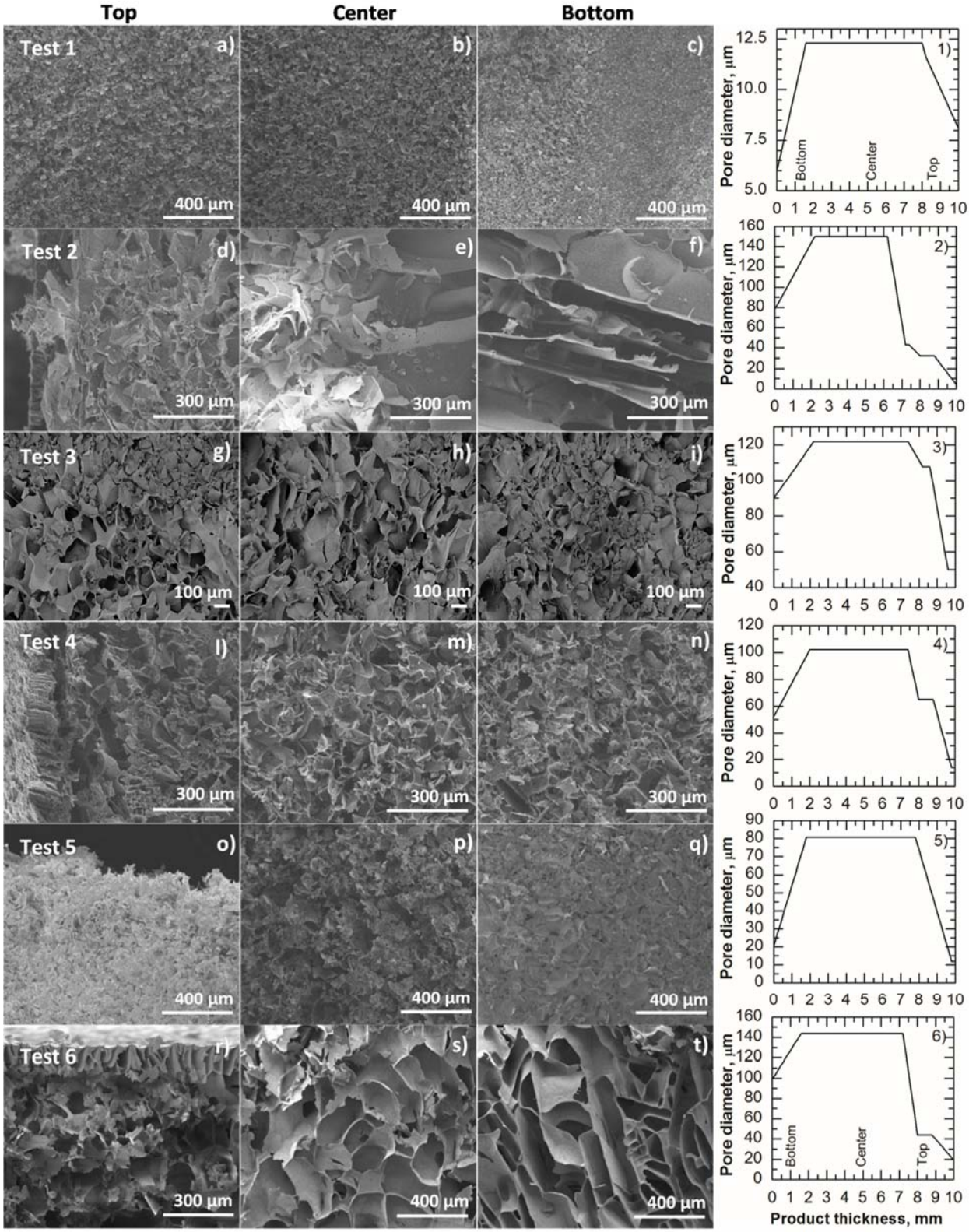
Top
Center
Bottom
Test 1
a)
b)
c)
400 µm
Test 2
d)
e)
f)
300 µm
Test 3
g)
h)
i)
100 µm
Test 4
l)
m)
n)
300 µm
Test 5
o)
p)
q)
400 µm
Test 6
r)
s)
t)
300 µm
400 µm
Pore diameter, µm
1)
2)
3)
4)
5)
6)
Bottom
Center
Top
Product thickness, mm

Figure 6

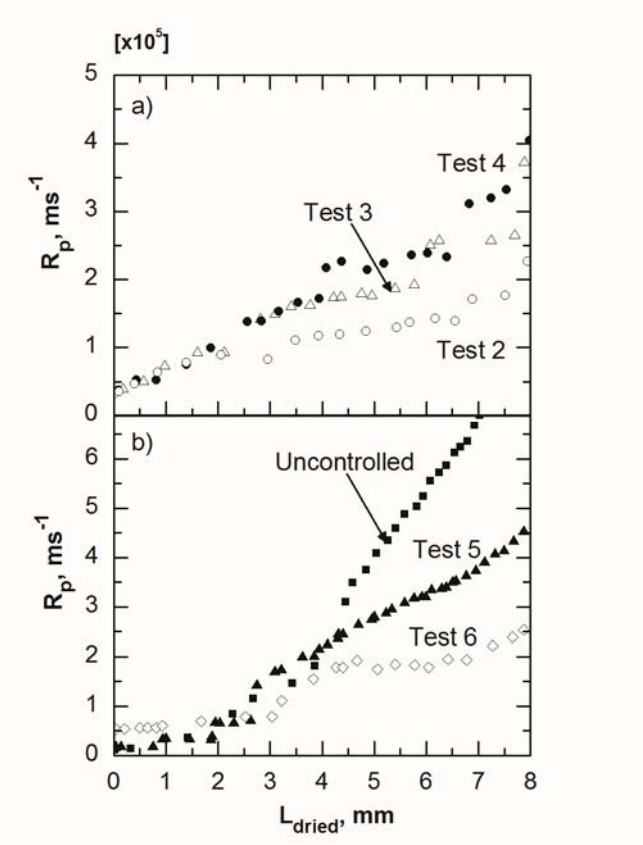
[x10^5]
a)
Test 4
Test 3
Test 2
R_p, ms^-1
b)
Uncontrolled
Test 5
Test 6
R_p, ms^-1
L_dried, mm

Figure 7

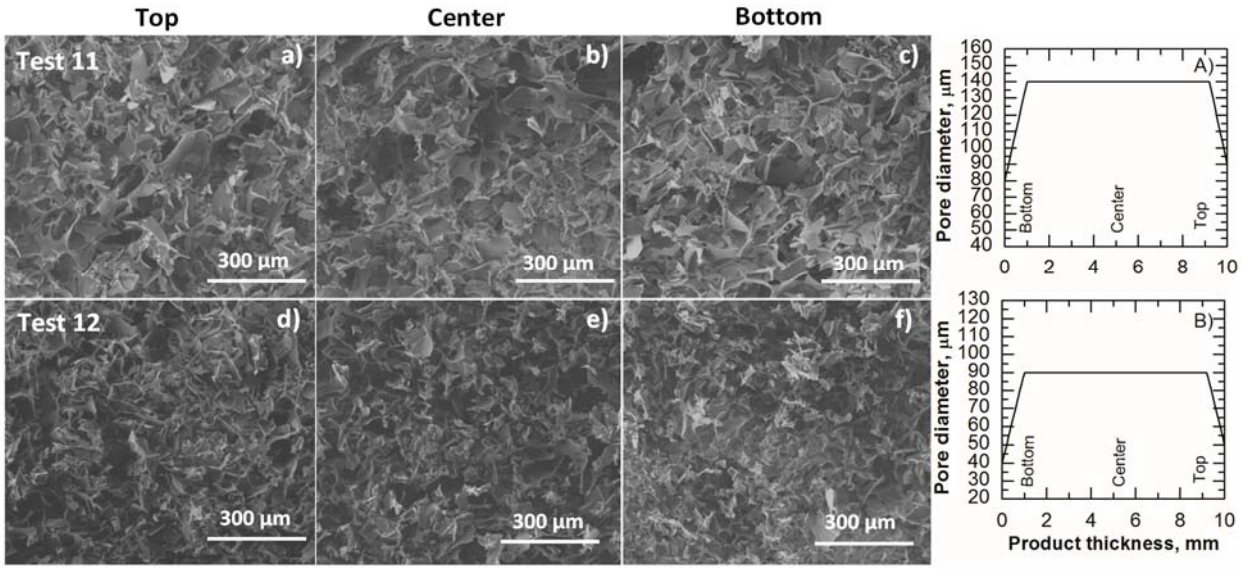
Top
Center
Bottom
Test 11
a)
b)
c)
300 µm
Test 12
d)
e)
f)
A)
B)
Pore diameter, µm
Bottom
Center
Top
Product thickness, mm

Figure 8

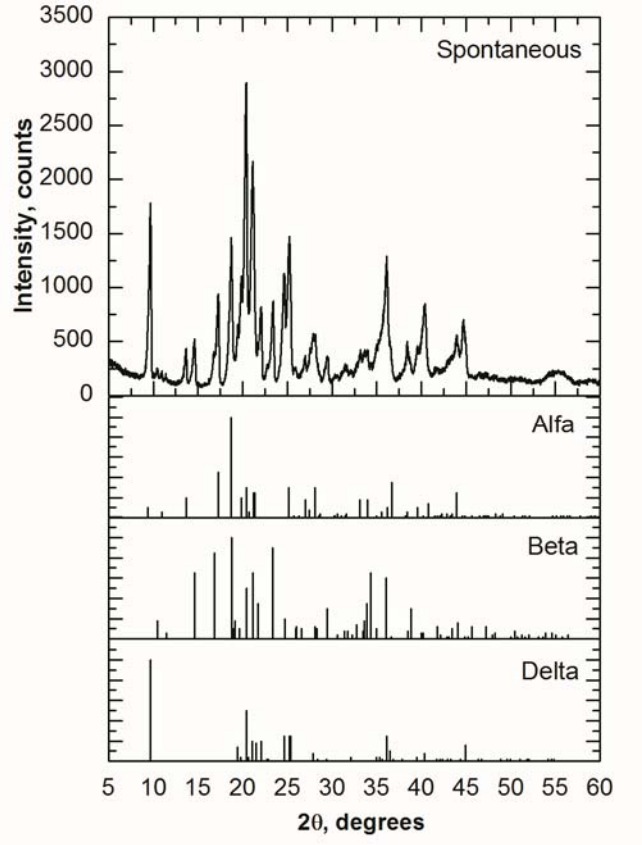
Spontaneous
Alfa
Beta
Delta
Intensity, counts
3500
3000
2500
2000
1500
1000
500
0
5 10 15 20 25 30 35 40 45 50 55 60
2θ, degrees

Figure 9

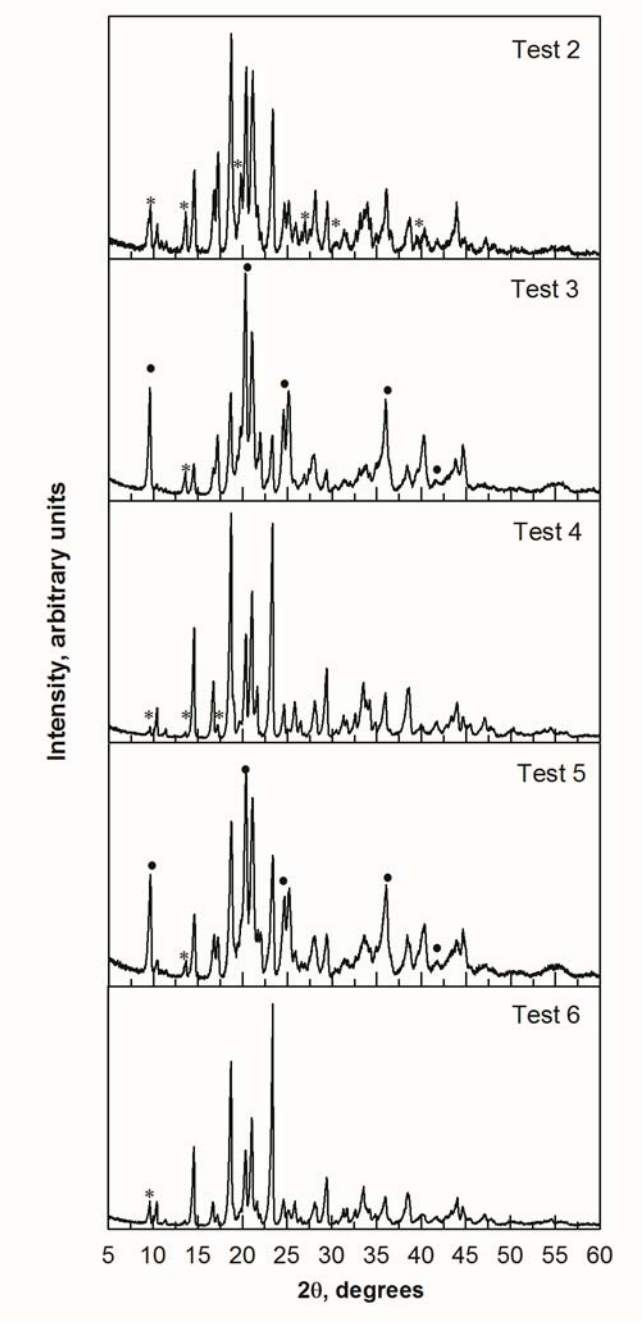
Test 2
Test 3
Test 4
Test 5
Test 6
Intensity, arbitrary units
5 10 15 20 25 30 35 40 45 50 55 60
2θ, degrees

Figure 10

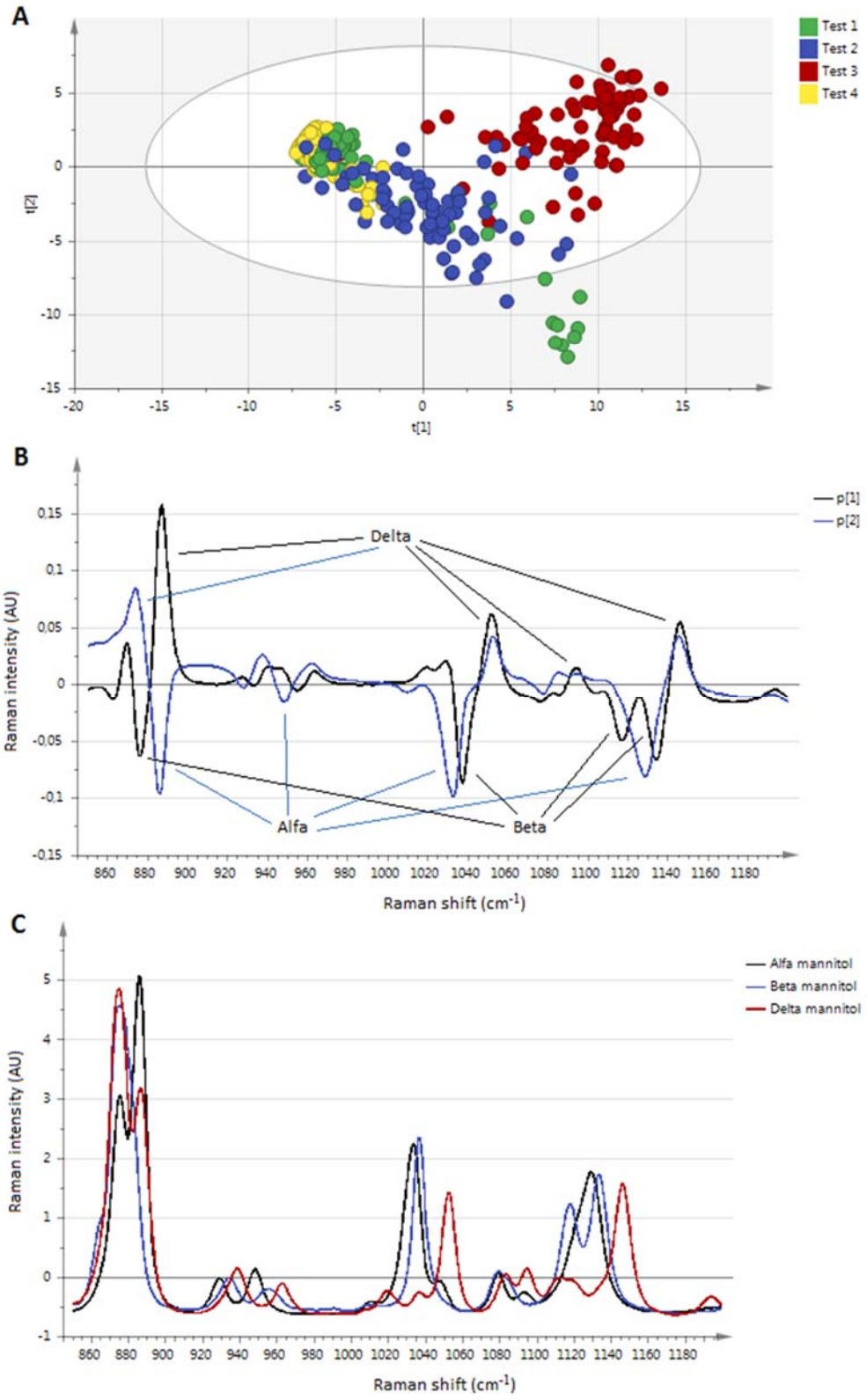
A
Test 1
Test 2
Test 3
Test 4
t[2]
t[1]
B
p[1]
p[2]
Delta
Alfa
Beta
Raman intensity (AU)
Raman shift (cm-1)
C
Alfa mannitol
Beta mannitol
Delta mannitol
Raman intensity (AU)
Raman shift (cm-1)